HAL
open science

Theoretical and Experimental Analysis of Asymmetrically Clipped-FSK VLC System

Muhammad Jehangir Khan, Ali Azim, Yannis Le Guennec, Ghislaine Maury, Laurent Ros

To cite this version:

Muhammad Jehangir Khan, Ali Azim, Yannis Le Guennec, Ghislaine Maury, Laurent Ros. Theoretical and Experimental Analysis of Asymmetrically Clipped-FSK VLC System. IEEE Photonics Journal, 2022, 14 (3), pp.1-9. 10.1109/JPHOT.2022.3165439 . hal-03662332

HAL Id: hal-03662332

https://hal.science/hal-03662332v1

Submitted on 9 May 2022

HAL is a multi-disciplinary open access archive for the deposit and dissemination of scientific research documents, whether they are published or not. The documents may come from teaching and research institutions in France or abroad, or from public or private research centers.

L'archive ouverte pluridisciplinaire **HAL**, est destinée au dépôt et à la diffusion de documents scientifiques de niveau recherche, publiés ou non, émanant des établissements d'enseignement et de recherche français ou étrangers, des laboratoires publics ou privés.

Theoretical and Experimental Analysis of Asymmetrically Clipped-FSK VLC System

Muhammad Jehangir Khan, Ali W. Azim, Yannis Le Guennec, Ghislaine Maury and Laurent Ros .

***Abstract*—In this article, energy efficient asymmetrically clipped frequency-shift keying (AC-FSK) based visible light communication (VLC) system is theoretically and experimentally demonstrated. In order to facilitate straightforward comparison with the experimental results, theoretical expression for bit error probability, based on the Euclidean distance analysis of AC-FSK symbols, is provided. The VLC setup is based on commercial off-the-shelf components and software defined radio. The bit error rate (BER) performance of AC-FSK is evaluated considering maximum likelihood (ML) receiver, 1-tap discrete cosine transform (DCT) based receiver and frequency-domain harmonic receiver. Simulation and experimental results reveal that the performance of harmonic and ML receivers is almost identical. On the other hand, considering harmonic receiver for both AC-FSK and state-of-the-art unipolar (U)-FSK, we also gather that the BER performance of both schemes is almost the same. However, the harmonic receiver complexity of AC-FSK is 41.6% and 33.3% less compared to that of U-FSK for modulation order $M = 16$ and $M = 128$, respectively. This is because unlike U-FSK, AC-FSK requires limited number of harmonics for its optimal operation.**

***Index Terms*—Frequency-shift keying, visible light communication, intensity modulation and direct detection, energy efficient modulation.**

I. Introduction

Visible light communication (VLC) is a promising technology to alleviate the scarcity problem of radio-frequency (RF) spectral resources [1]. Extensive research has been carried out on high data rate intensity modulation direct-detection (IM-DD) VLC systems [2] which may employ spectral efficient modulations, such as pulse-amplitude modulation (PAM) [3] or optical-orthogonal frequency-division multiplexing (O-OFDM) [4]. Nonetheless, VLC can also be used for reliable and energy efficient low data rate (100 kbps to 1 Mbps) applications [5]. It may be noticed that for low data rate energy efficient applications, classical linear modulations like PAM and O-OFDM may not be suitable choices because of their poor energy efficiency which negatively impacts the autonomy of battery powered terminals. On the other hand, non-linear modulations [6], for which, the energy efficiency is improved by decreasing the spectral efficiency, i.e., increasing alphabet cardinality, could be promising candidates. Among these non-linear modulations, pulse-position modulation (PPM) has been extensively studied [7] [8], and experimentally demonstrated for VLC [9]. However, PPM has some serious limitations, such as: (i) synchronization issues at the receiver; (ii) strong multi-path channel impact on bit error rate (BER) performance; and (iii) high peak to average power ratio [10]-[11]. In order to circumvent these limitations of PPM, frequency-shift keying (FSK) has been proposed for energy efficient RF systems [12]-[13]. However, for IM-DD implementation of VLC systems, FSK needs to be substantially modified to deal with the unipolar and real-valued constraints on the transmit signal imposed by IM-DD [10], [14]. In [10], a unipolar variant of FSK, referred to as unipolar (U)-FSK is proposed. The basic idea of U-FSK is to transmit the positive amplitude excursions and sign flipped negative amplitude excursions in two consecutive symbol periods. Simulation results reveal that U-FSK is energy efficient relative to on-off keying (OOK) and PAM [10]. Moreover, its energy efficiency improves by increasing the alphabet cardinality. However, the maximum likelihood (ML) receiver of U-FSK has a high computational complexity. Thus, in order to reduce the receiver complexity, a frequency-domain harmonic receiver for U-FSK has been proposed in [15] whose performance is close to that of ML receiver. The complexity of the harmonic receiver is significantly reduced compared to the time-domain (TD) ML receiver, due to the simplified correlation computation between the frequency-domain received signal and frequency-domain waveforms from dictionary, considering limited number of taps for correlation computation. From this frequency-domain approach, we also observed that only two harmonics are needed for optimal detection of odd U-FSK frequencies, whereas twelve harmonics are required for optimal detection of even frequencies. This led to the proposal of asymmetrically clipped (AC)-FSK, where only odd frequencies are used (while transmitting only the positive amplitude excursions, and not the sign flipped negative amplitude ones) to reduce the harmonic receiver complexity [16]. Simulation results depict that harmonic receiver based AC-FSK exhibits similar BER as harmonic receiver based U-FSK, for the same spectral efficiency. However, as aforementioned, the complexity of AC-FSK harmonic receiver is significantly reduced relatively to U-FSK harmonic receiver as it only uses odd frequencies which requires lower number of harmonics for optimal performance.

Against the given background, the contributions of this article are as follows:

- Firstly, we provide an expression which evaluates the

Muhammad Jehangir Khan, Yannis Le Guennec and Laurent Ros are with Université Grenoble Alpes, CNRS, Grenoble INP, GIPSA-LAB, 38000 Grenoble, France (email: {Muhammad-Jehangir.Khan, yannis.leguennec, laurent.ros}@gipsa-lab.grenoble-inp.fr). Ghislaine Maury is with Université Grenoble Alpes, CNRS, Grenoble INP, IMEP-LAHC, 38000 Grenoble, France (email: maury@grenoble-inp.fr).

Ali W. Azim is with Department of Telecommunication Engineering, University of Engineering and Technology, Taxila, Pakistan (email: ali-waqarazim@gmail.com)

minimum Euclidean distance for AC-FSK dictionary. This expression permits to derive an approximate theoretical expression using which the bit error probability for AC-FSK can be obtained. This theoretical bit error probability expression will be used as benchmark to analyze the performance of different receivers for AC-FSK.

- Detailed receiver architectures are presented which were not presented in [16].
- We validate the proof-of-concept of AC-FSK (considering both ML and harmonic receiver) by experimentally demonstrating its performance over a VLC test-bench. The experimental BER performance of AC-FSK is also compared with that of U-FSK. It shall become evident that practical implementation of AC-FSK is feasible and makes it a viable alternative for low data rate energy efficient VLC.

A. Notations

Unless otherwise mentioned, lower-case boldface italic letters represent the discrete time-domain vectors, e.g., $\boldsymbol{s}_m$, where m in subscript indicates the activated frequency. The nth sample of $\boldsymbol{s}_m$ is given as $\boldsymbol{s}_m[n]$. The frequency-domain counterparts of the discrete time-domain waveforms are denoted by the upper-case boldface italic letters, e.g., $\boldsymbol{S}_m$. The kth frequency component of $\boldsymbol{S}_m$ is given as $S_m[k]$. Boldface caligraphic letters denote the matrices, e.g., $\boldsymbol{\mathcal{D}}$. The operations such as transpose, inner product, convolution, absolute value and Euclidean norm are respectively represented by $(\cdot)^{\mathrm{T}}$, $\langle\cdot,\cdot\rangle$, $\otimes$, $|\cdot|$ and $\|\cdot\|$.

B. Paper Organization

In Section II, AC-FSK signaling is revisited, whereby, the time-domain and frequency-domain waveforms and its receiver architectures are presented in detail. Moreover, the Euclidean distance analysis for AC-FSK symbols is also presented in the same section. In Section III, a theoretical expression of AC-FSK bit error probability as a function of received optical power is derived and is compared with simulation results from [16]. In Section IV, the VLC experimental set-up is presented and experimental BER results are reported for AC-FSK for different receiver architectures. Based on the experimental and theoretical results obtained by comparing the performance of AC-FSK with other counterparts, the conclusions are rendered in Section V.

II. M-ary AC-FSK Signaling

A. M-ary AC-FSK Waveform Analysis

1) Time-Domain Waveforms: M-ary AC-FSK is proposed in [16]. The dictionary of possible M waveforms for AC-FSK is derived from the classical bipolar $2M$-ary FSK dictionary. The discrete-time samples, $\tilde{s}_k[n]$ of the the kth frequency FSK waveform, $\tilde{\boldsymbol{s}_k}$ of the $2M$-ary FSK dictionary are given as:

$$\tilde{s}_k[n] = \begin{cases} \frac{A}{\sqrt{2}} & k = 0 \\ A\cos\left(\pi k \frac{2n+1}{4M}\right) & 1 \leq k \leq 2M-1 \end{cases}, \quad (1)$$

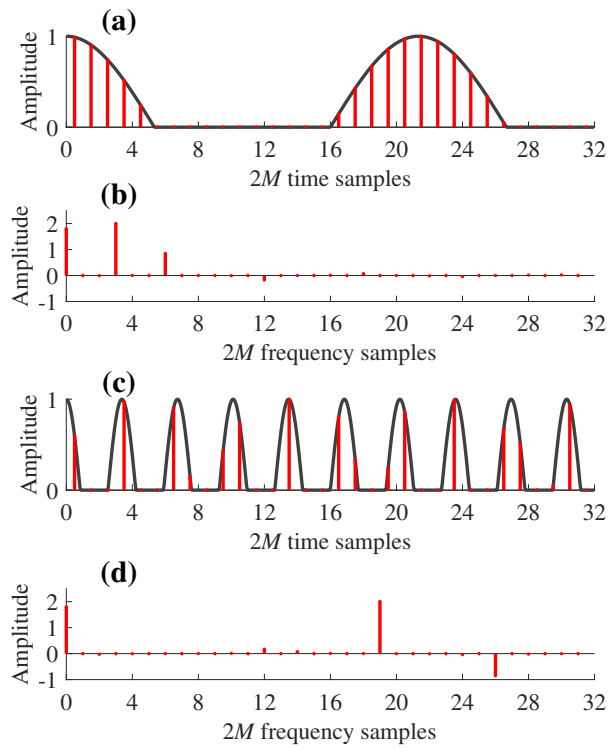

Fig. 1: Discrete time-domain AC-FSK waveforms for $m = 2$ (a) and $m = 10$ (c), frequency-domain waveforms for $m = 2$ (b) and $m = 10$ (d), considering $M = 16$.

where $0 \leq n \leq 2M-1$ and A is the waveform amplitude. The waveform (i.e symbol) duration is $\tilde{T}_s = M_c T_c$, where T_c is the chip duration, and M_c is the number of chips per waveform, $M_c = 2M$ when no oversampling is considered. The minimum frequency separation between adjacent waveforms frequencies to ensure orthogonality is $\Delta f = 1/2\tilde{T}_s$ [10]. To build the AC-FSK dictionary, $\boldsymbol{\mathcal{D}}^{\mathrm{AC}}$ having cardinality M, only the odd frequency waveforms from $\boldsymbol{\mathcal{D}}^{2\mathrm{M-FSK}}$ are extrapolated and their negative samples are clipped to zero to comply with the IM-DD constraints. Thus, the discrete-time mth AC-FSK waveform, i.e., having mth frequency is defined as:

$$s_m[n] = \tilde{s}^{+}_{k_{\mathrm{odd}}}[n] = \begin{cases} \tilde{s}_{k_{\mathrm{odd}}}[n] & \tilde{s}_{k_{\mathrm{odd}}}[n] \geq 0 \\ 0 & \tilde{s}_{k_{\mathrm{odd}}}[n] < 0 \end{cases} \quad (2)$$

for $m \in \{1, 2, \cdots, M\}$ and $k_{\mathrm{odd}} = 2m-1$, and then $k_{\mathrm{odd}} \in \{1, 3, \cdots, 2M-3, 2M-1\}$. Considering a fixed chip duration, T_c, the symbol duration of mth AC-FSK symbol, $\boldsymbol{s}_m = [s_m[0], \cdots, s_m[2M-1]]^{\mathrm{T}}$ is $T_s = \tilde{T}_s$.

2) Frequency-Domain Waveforms: $2M$-order discrete cosine transform (DCT) is applied on AC-FSK symbol, $\boldsymbol{s_m}$ to attain its frequency-domain counterpart, $\boldsymbol{S}_m$ as:

$$\boldsymbol{S}_m = \boldsymbol{\mathcal{C}}_{2M}\boldsymbol{s}_m, \quad (3)$$

where $\boldsymbol{\mathcal{C}}_{2M}$ is the $2M$-order DCT matrix as in [16] and $\boldsymbol{S}_m$ in vectorial form is given as $\boldsymbol{S}_m = [S_m[0], \cdots, S_m[2M-1]]^{\mathrm{T}}$.

Let us consider that the mth AC-FSK frequency is activated, i.e., we have $\boldsymbol{s}_m$, then its frequency-domain counterpart, i.e., $\boldsymbol{S}_m$, will show: (i) a DC component, (ii) one harmonic related

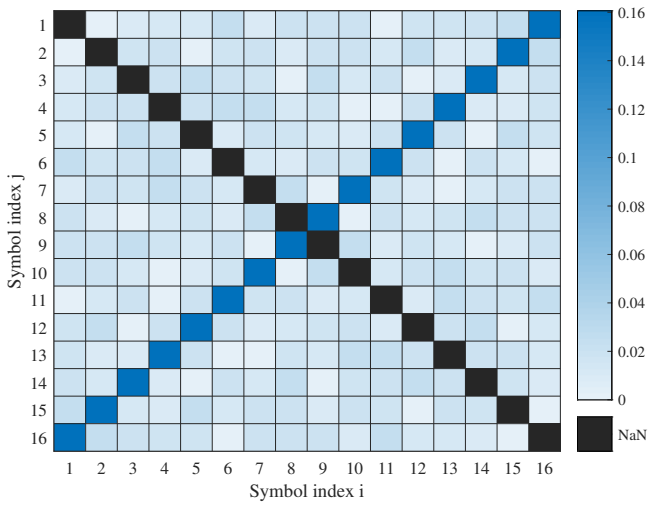

Fig. 2: Deviation, Δ of the squared Euclidean distance between different symbol pairs, $d^2_{i,j}$ with $i \neq j$, relatively to the minimum squared Euclidean distance, $d^2_{\min}$. NaN: not a number.

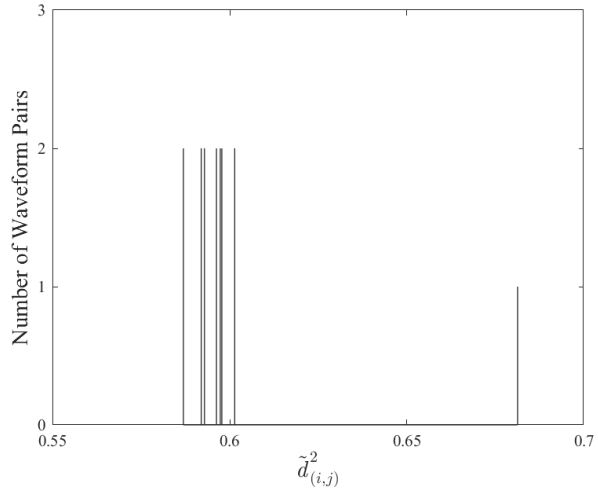

Fig. 3: Histogram of the squared normalized distances, i.e., $\tilde{d}^2_{i,j} = d^2_{i,j}/2E_{\mathrm{s(elec)}}$ for 16-ary AC-FSK. Squared normalized distance, $\tilde{d}^2_{i,j}$ between one waveform with the whole dictionary, $\mathcal{D}^{\mathrm{AC}}$ is presented.

to the fundamental (activated) frequency with index $2m-1$ and amplitude $2A$, and (iii) even order harmonics carrying the distortion due to the clipping operation. The amplitudes of the even $2p$th harmonics, S^{2p}_m are given as:

$$S^{2p}_m = \frac{8A}{\pi}\frac{(-1)^p}{1-4p^2}, \tag{4}$$

with $p \in \mathbb{N}^*$. For $0 \leq m \leq M/2-1$, second harmonic ($p=1$ in (4)) is located at index $4m-2$, i.e., $S_m[4m-2] = 8A/3\pi$. For $M/2 < m \leq M-1$, second harmonic is aliased at index $4M-4m+2$, i.e., $S_m[4M-4m+2] = -8A/3\pi$.

Considering $M=16$, $m=2$ and $m=10$, Fig. 1 shows the discrete time-domain (cf. Fig. 1 (a) and (c)) and frequency-domain (Fig. 1 (b) and (d)) representations of $\boldsymbol{s}_m$ and $\boldsymbol{S}_m$, respectively. The amplitudes of the harmonics illustrated in Fig. 1 (b) and (d), which are obtained from numerical DCT computations, are consistent with (4), considering $A=1$. It is highlighted that the fundamental and second harmonic contain more than 99% of AC-FSK symbol energy, discarding the DC component.

The baseband modulation bandwidth (without taking into account clipping distortion harmonics [17]), is $B = 2M\Delta f$. As bit rate is expressed as $R_{\mathrm{b}} = \log_2(M)/\tilde{T}_s$, M-ary AC-FSK spectral efficiency, η is defined as:

$$\eta = \frac{R_b}{B} = \frac{\log_2(M)}{M}. \tag{5}$$

B. Euclidean Distance between AC-FSK symbols

All the waveforms in $\boldsymbol{\mathcal{D}}^{\mathrm{AC}}$ have the same average electrical symbol energy, $E_{\mathrm{s(elec)}} = (A^2/4)T_s$. The minimum squared Euclidean distance between any waveform pairs $(\boldsymbol{s}_i;\ \boldsymbol{s}_j)$ of $\boldsymbol{\mathcal{D}}^{\mathrm{AC}}$, with $i \neq j$, is defined as:

$$\begin{aligned} d^2_{\min} &= \min_{i\neq j} d^2_{i,j} = \min_{i\neq j} \|\boldsymbol{s}_i - \boldsymbol{s}_j\|^2 \\ &= \min_{i\neq j}\Big\{2E_{\mathrm{s(elec)}} - 2\langle \boldsymbol{s}_i, \boldsymbol{s}_j\rangle\Big\}. \end{aligned} \tag{6}$$

It may be observed that the inner products, $\langle \boldsymbol{s}_i, \boldsymbol{s}_j\rangle$ for $i \neq j$ is not zero because of the orthogonality loss due to the clipping process. Henceforth, it is mandatory to find the waveform pair, $(\boldsymbol{s}_i;\ \boldsymbol{s}_j)$ that has maximum inner product which shall result in the minimum squared Euclidean distance (6). Mathematical analysis indicates that the maximum value for $\langle \boldsymbol{s}_i, \boldsymbol{s}_j\rangle$ is achieved for $i=1$ and $j=2$, which leads to:

$$\begin{aligned} d^2_{\min} &= \frac{A^2 T_s}{2}\left[1 - \frac{3\sqrt{3}}{4\pi}\right] \\ &= 2E_{\mathrm{s(elec)}}\gamma^{\mathrm{AC}}, \end{aligned} \tag{7}$$

where $\gamma^{\mathrm{AC}} = (1 - 3\sqrt{3}/4\pi) \approx 0.59$ is a penalty factor on the minimum distance induced by orthogonality loss. Penalty factors for M-ary U-FSK and M-ary DC-FSK are $\gamma^{\mathrm{U}} = 0.55$ and $\gamma^{\mathrm{DC}} = 0.33$, respectively [10]. Note that, the higher the value of the penalty factor γ, the higher the energy efficiency relatively to conventional M-ary FSK (no degradation if $\gamma = 1$).

For clarity, we evaluate the deviation of the squared Euclidean distance for all symbol pairs, $d^2_{i,j}$ with $i \neq j$ relative to $d^2_{\min}$, by defining the parameter Δ as:

$$\Delta = \frac{d^2_{i,j} - d^2_{\min}}{d^2_{\min}}. \tag{8}$$

Fig. 2 represents a heat-map of Δ as a function of all possible waveform pairs $(\boldsymbol{s}_i;\ \boldsymbol{s}_j)$, considering 16 AC-FSK. It can be seen from Fig. 2 that the squared Euclidean distance between any symbol pairs does not deviate more than 16.06% from $d^2_{\min}$ for $M = 16$. For higher modulation alphabet cardinalities, e.g., $M = 1024$, the deviation from $d^2_{\min}$ is not more than 16.23%. Fig. 3 illustrates the histogram of the normalized squared Euclidean distance for M-ary AC-FSK, considering $M = 16$, i.e., $\tilde{d}^2_{i,j} = d^2_{i,j}/2E_{\mathrm{s(elec)}}$, where $d^2_{i,j} = \|s_i(t) - s_j(t)\|^2$ is the squared Euclidean distance between waveform pairs $(\boldsymbol{s}_i;\ \boldsymbol{s}_j)$ in the dictionary, $\mathcal{D}^{\mathrm{AC}}$ for

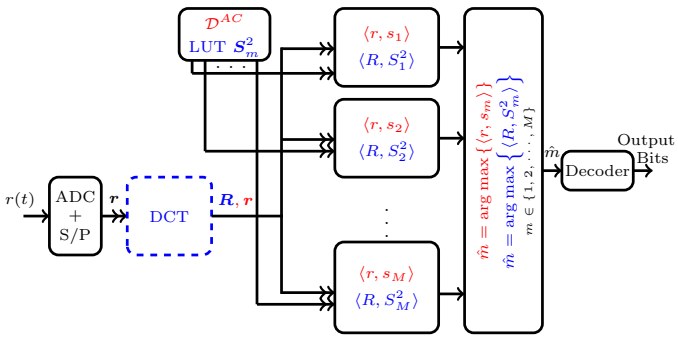

Fig. 4: Optimal ML TD receiver (red/black) and 2-tap harmonic receiver (blue/black) structure for M-ary AC-FSK.

$i \neq j$. For a given symbol s_i, 15 symbol pairs are considered in Fig. 3. It can be seen in Fig. 3 that most of the waveform pairs $(\boldsymbol{s}_i; \boldsymbol{s}_j)$ have squared Euclidean distances close to $d^2_{\min}$, for which $d^2_{\min}/2E_{s(elec)}$=$\gamma^{\mathrm{AC}} \approx 0.59$, while there is one symbol $\boldsymbol{s}_j$ which shows a squared Euclidean distance related to s_i which is significantly larger than $d^2_{\min}$.

C. Channel Model

The received waveform $\boldsymbol{r}$, contaminated by the ambient noise, $\boldsymbol{w}$ is given as:

$$\boldsymbol{r} = \boldsymbol{s}_m + \boldsymbol{w}, \tag{9}$$

where $\boldsymbol{w}$ is an additive white Gaussian noise (AWGN) having mono-lateral power spectral density (PSD) of N_0. For clarity of exposition, $\boldsymbol{w}$ and $\boldsymbol{r}$ in vectorial form are given as $\boldsymbol{w} = [w[0], \cdots, w[2M-1]]^{\mathrm{T}}$ and $\boldsymbol{r} = [r[0], \cdots, r[2M-1]]^{\mathrm{T}}$.

D. M-ary AC-FSK Receivers

1) Optimal Time-Domain Receiver: Considering that all waveforms in $\boldsymbol{\mathcal{D}}^{\mathrm{AC}}$ are equiprobable, i.e., $p(\boldsymbol{s}_m) = 1/M$ and have equal energy, i.e., $E_{\mathrm{s(elec)}}$, then the theoretical time-domain maximum likelihood (TD ML) receiver identifies $\boldsymbol{s}_m \in \boldsymbol{\mathcal{D}}^{\mathrm{AC}}$ which maximizes the likelihood function, $p(\boldsymbol{r}|\boldsymbol{s}_m)$. Note that $p(\boldsymbol{r}|\boldsymbol{s}_m)$ is the conditional probability of receiving $\boldsymbol{r}$ when $\boldsymbol{s}_m$ is sent. Considering an AWGN channel having noise variance $\sigma^2 = N_o B$, the likelihood function is given as:

$$\begin{aligned} p(\boldsymbol{r}|\boldsymbol{s}_m) &= \left(\frac{1}{2\pi\sigma^2}\right)^{M_c} \exp\left(-\frac{\|\boldsymbol{r}-\boldsymbol{s}_m\|^2}{2\sigma^2}\right) \\ &= \Lambda \exp\left(\frac{\langle \boldsymbol{r}, \boldsymbol{s}_m \rangle}{\sigma^2}\right). \end{aligned} \tag{10}$$

Here, $\Lambda = (1/2\pi\sigma^2)^{M_c} \exp(-\|\boldsymbol{r}\|^2 - \|\boldsymbol{s}_m\|^2/2\sigma^2)$ which follows from the fact that $\|\boldsymbol{r}-\boldsymbol{s}_m\|^2 = \|\boldsymbol{r}\|^2 + \|\boldsymbol{s}_m\|^2 - 2\langle \boldsymbol{r}, \boldsymbol{s}_m \rangle$. Then, the estimated activated frequency, $\hat{m}$ using theoretical TD ML receiver can be identified as:

$$\hat{m} = \arg\max_m \langle \boldsymbol{r}, \boldsymbol{s}_m \rangle, \quad m \in \{1, 2, ..., M\}. \tag{11}$$

The receiver architecture for the optimal TD ML receiver for M-ary AC-FSK is illustrated in Fig. 4, where necessary operations are identified using (red/black).

2) 1-tap DCT-based Receiver: It is evident that the computational complexity of the TD ML receiver is very high; which makes it less practical. However, it is possible to simplify the factor $\langle \boldsymbol{r}, \boldsymbol{s}_m \rangle$ in (11), which leads to a low-complexity sub-optimal receiver. In this perspective, the factors;

$$\langle \boldsymbol{r}, \boldsymbol{s}_m \rangle = \langle \boldsymbol{r}, \tilde{s}^{+}_{2m-1} \rangle \tag{12}$$

for $m \in \{1, 2, ..., M\}$ (see (11), (2)), are simply replaced by inner products with the bi-polar FSK waveforms

$$\langle \boldsymbol{r}, \tilde{\boldsymbol{s}}_{2m-1} \rangle = R[2m-1], \tag{13}$$

that can be obtained by the DCT of $\boldsymbol{r}$ evaluated at odd frequency index $2m-1$. Indeed, $R[2m-1]$ represents the $2m-1^{th}$ component of the DCT vector :

$$\boldsymbol{R} = \boldsymbol{\mathcal{C}}_{2M}\boldsymbol{r} = [R[0], \cdots, R[2M-1]]^{\mathrm{T}}. \tag{14}$$

The activated frequency index, m is then identified as:

$$\hat{m} = \arg\max_m \Big\{R[2m-1]\Big\}, \quad m \in \{1, 2, ..., M\}. \tag{15}$$

Thus, essentially the decision on the activated frequency is taken on 1-tap of $\boldsymbol{R}$ which exhibits the maximum amplitude. The sub-optimality of 1-tap DCT-based receiver is due to the fact that it completely ignores the clipping distortion falling on even frequencies, since DCT output is only considered for odd frequencies (15). In other words, knowing from (2) that AC-FSK symbol is the half sum of one FSK-symbol (pure tone) plus its absolute value (even harmonics), $s_m[n] = \frac{1}{2}(\tilde{s}_{2m-1}[n] + |\tilde{s}_{2m-1}[n]|)$, the 1-tap DCT-based receiver is only matched to the first component of the symbol, ignoring fully the second component.

3) 2-tap Harmonic Receiver: The idea behind the 2-tap harmonic receiver is to include the clipping distortion harmonics which were not considered for the low-complexity sub-optimal receiver to identify the activated frequency. Fig. 4 (blue/black) illustrates the architecture of the 2-tap harmonic receiver for M-ary AC-FSK. In the first (off-line) step, the two most significant harmonics (leaving aside the DC component) are selected from (4) to build a dictionary of M waveforms, $\boldsymbol{S}^2_m$, which are then interpolated in a look-up-table (LUT). In a second (on-line) step, $2M$-order DCT is applied on $\boldsymbol{r}$ to obtain $\boldsymbol{R}$. Lastly, the frequency-domain cross-correlation is evaluated between $\boldsymbol{R}$ and $\boldsymbol{S}^2_m$ to identify the transmit frequency index, $\hat{m}$ as [16]:

$$\hat{m} = \arg\max_m \langle \boldsymbol{R}, \boldsymbol{S}^2_m \rangle, \quad m \in \{1, 2, ..., M\}, \tag{16}$$

where the factor $\langle \boldsymbol{R}, \boldsymbol{S}^2_m \rangle$ can be explicitly expressed as:

$$\langle \boldsymbol{R}, \boldsymbol{S}^2_m \rangle = R[2m-1].S_m[2m-1] + R[k_{2nd}].S_m[k_{2nd}], \tag{17}$$

with k_{2nd} the index of the second harmonic (even) frequency ($k_{2nd} = 2 \times (2m-1)$ if $m < M/2$, or $2 \times (2M - (2m-1))$ if $m \geq M/2$ (see section II-A2)).

The harmonic receiver can be regarded as a 2-taps DCT based receiver, with the same front-end as 1-tap DCT based receiver. However, the 2-taps recombination $\langle \boldsymbol{R}, \boldsymbol{S}^2_m \rangle$ in (17)(16) permits to approach closely $\langle \boldsymbol{R}, \boldsymbol{S}_m \rangle$ (frequency formulation),

TABLE I: Complexity computations and complexity reduction, β for 2-tap harmonic receiver relative to the optimal TD ML receiver, considering different M, for M-ary AC-FSK.

M	$\mathcal{C}_{\mathrm{TD,ML}}$	$\mathcal{C}_{\mathrm{harm}}$	β (%)
16	256	112	56.3
32	1024	256	75.0
64	4096	576	85.9
128	16384	1280	92.2
256	65536	2816	95.7
512	262144	6144	97.7

which is equal to the inner product $\langle \boldsymbol{r}, \boldsymbol{s}_m \rangle$ (time formulation) appearing in the optimal time-domain receiver (11). Hence, the performance of the 2-tap harmonic receiver is expected to be close to the one of the optimal time-domain receiver.

4) Complexity Analysis: We have observed that the primary contributor to the receiver complexity is the number of multiplications required to identify the frequency, whereas, the number of additions is not significant when calculating the overall receiver complexity. Therefore, the complexities of the receivers are computed by considering only the number of non-zero real multiplications.

The complexity (number of non-zero real multiplications) of the optimal TD ML receiver is $\mathcal{C}_{\mathrm{TD,ML}} = MM_{\mathrm{c}} = M^2$ because half of the chips of M-ary AC-FSK time-domain waveforms are clipped to zero [16]. For the sub-optimal receiver, only a $2M$-order DCT is needed, which requires $\mathcal{C}_{\mathrm{sub-opt}} = M\log_2(2M)$ multiplications [16]. Similarly, the 2-tap harmonic receiver requires $\mathcal{C}_{\mathrm{harm}} = M\log_2(2M) + 2M$ multiplications, which is slightly larger relative to 1-tap DCT receiver, but is still linearithmic with M [16]. This increase in the complexity of 2-tap harmonic receiver relative to the 1-tap DCT receiver is about 40% and 25% for $M = 16$ and 128, respectively.

The complexity of 2-tap harmonic receiver is drastically reduced compared to the optimal TD ML receiver. For clear understanding, we introduce β to evaluate the complexity reduction of the 2-tap harmonic receiver as compared to the optimal TD ML receiver for different M, i.e., $\beta = (1 - \mathcal{C}_{\mathrm{harm}}/\mathcal{C}_{\mathrm{TD,ML}}) \times 100\%$. In fact, β evaluates the percentage decrease in the complexity of the 2-tap harmonic receiver relative to the optimal TD ML receiver for different M. In Tab. I, the complexity computations of optimal TD ML and 2-tap harmonic receivers for M-ary AC-FSK and the complexity reduction β are provided for different M.

It is recalled that the complexity of $(12, 2)$-tap harmonic receiver for M-ary U-FSK [15] is $\mathcal{C}^{\mathrm{U}}_{\mathrm{harm}} = M\log_2(2M) + L_e(M/2) + L_o(M/2)$, where $L_e = 12$ and $L_o = 2$ are the number of taps selected for even and odd frequencies, respectively. It is found that the complexity reduction of 2-tap harmonic receiver for M-ary AC-FSK relative to $(12, 2)$-tap harmonic receiver for M-ary U-FSK is about 41.6% and 33.3% for $M = 16$ and $M = 128$, respectively.

In the next sections, we shall demonstrate theoretically and experimentally that the harmonic receiver based M-ary AC-FSK overcomes the energy efficiency versus complexity trade-off that exists in the optimal TD ML and 1-tap DCT-based receivers. Moreover, harmonic receiver based M-ary AC-FSK is expected to reach slightly improved energy efficiency than M-ary U-FSK but with a significantly reduced complexity.

III. Bit Error Probability for AC-FSK

A. Average Optical Energy per Bit

To evaluate the theoretical performance of AC-FSK to serve as a benchmark for simulation and experimental results, we express the bit error probability as a function of optical signal-to-noise ratio (SNR) per bit, i.e., $E_{\mathrm{b(opt)}}/N_0$ [18]. The optical energy per bit, $E_{b(opt)}$ can be defined from optical power, $P_{(opt)} = 1/M_c \sum_{n=0}^{M_c-1} |s_m[n]|$, i.e., $E_{b(opt)} = P_{(opt)}T_b$, where $T_b = T_s/\log_2(M)$ is the bit time. According to M-ary AC-FSK waveform definition in (2), $E_{\mathrm{b(elec)}}$ and $E_{\mathrm{b(opt)}}$ are expressed as:

$$E_{\mathrm{b(elec)}} = \frac{A^2 T_b}{4} \quad \text{and} \quad E_{\mathrm{b(opt)}} = \frac{AT_b}{\pi}. \tag{18}$$

Using expression (7) $d^2_{\min} = 2E_{\mathrm{s(elec)}}\gamma^{\mathrm{AC}}$ with $E_{\mathrm{s(elec)}} = \log_2(M)E_{\mathrm{b(elec)}}$, and incorporating (18) into (7), an expression relating $d^2_{\min}$ to $E_{\mathrm{b(opt)}}$ is obtained as:

$$d^2_{\min} = \Gamma E^2_{\mathrm{b(opt)}}, \tag{19}$$

where $\Gamma = \pi^2\gamma^{\mathrm{AC}}R_{\mathrm{b}}\log_2(M)/2$. It should be noticed that all the results of this article are given in terms of $E_{b(opt)}/N_o$, while complementary results in terms of $E_{b(elec)}/N_o$ are presented in [16].

B. Theoretical Bit Error Probability

The theoretical bit error probability expression for ML detection of conventional M-ary FSK in an AWGN channel is well known and demonstrated in [6], considering ML receiver. It is a function of the minimum Euclidean distance between FSK symbols, $d_{\min,\mathrm{FSK}}$. It has been demonstrated in Section II.B that the squared Euclidean distance between any pair of AC-FSK symbols does not deviate from $d^2_{\min}$ of more than 16.23% for $M \geq 16$. As a consequence, a relatively good approximation of theoretical symbol error probability, P_{e} can be obtained for AC-FSK with ML detection by substituting $d_{\min,\mathrm{FSK}}$ with $d_{\min}$ found for AC-FSK (19) in the FSK bit error probability expression [6], which leads to:

$$P_{\mathrm{e}} \approx \frac{M}{2\sqrt{2\pi}(M-1)} \int_{-\infty}^{+\infty} \left[1 - (1 - Q(x))^{M-1}\right] \times e^{\left[-\frac{\left(x - \sqrt{\Gamma \frac{E^2_{\mathrm{b(opt)}}}{N_0}}\right)^2}{2}\right]} \mathrm{d}x, \tag{20}$$

where $Q(\cdot)$ is the Gaussian Q-function [6], $e^{[\cdot]}$ is the exponential function.

C. Theoretical and Simulated Bit Error Probabilities

Fig. 5 illustrates Monte-Carlo simulation results for BER performance as a function of $E_{\mathrm{b(opt)}}/N_0$ for different M-ary AC-FSK receiver architectures including optimal TD ML

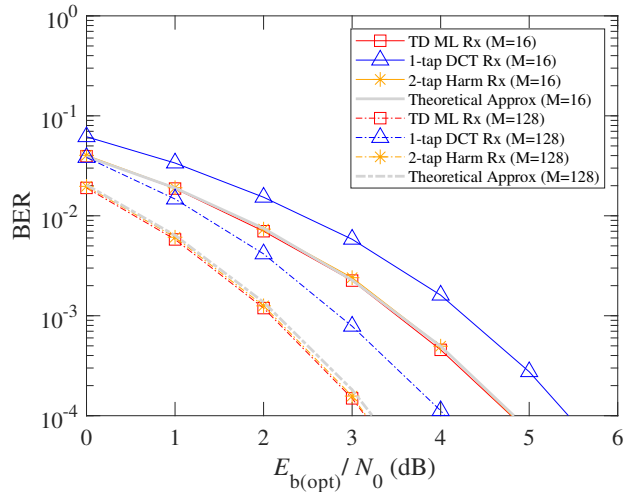

Fig. 5: Simulated and theoretical BER performance against $E_{\mathrm{b(opt)}}/N_o$ for M-ary AC-FSK receivers in AWGN channel considering $M = 16$ and $M = 128$. Average optical power is P_{opt}=1 W.

receiver (TD ML Rx), 1-tap DCT-based receiver (1-tap DCT Rx) and 2-tap harmonic receiver (Harm Rx), for an AWGN channel, considering $M = \{16, 128\}$ and a normalized average optical power $P_{(\mathrm{opt})}$ of 1W, which corresponds to $A = \pi$ in (18). The theoretical BER approximation given in (20) is also depicted in Fig. 5. The theoretical results are slightly worse ($i.e.$ have larger values) than the simulations because the theoretical bit error probability in (20) is based on the assumption that the distance between any waveform pairs $(\boldsymbol{s}_i;\ \boldsymbol{s}_j)$ with $i \neq j$ from the AC-FSK dictionary is $d_{\min}$ expressed in (19). Nevertheless, as demonstrated in Fig. 2 and discussed in section II.B, for a given transmitted symbol, one symbol pair has a distance significantly larger than $d_{\min}$. As a consequence, the theoretical bit error probability in (20) is slightly overestimated and acts as an upper bound for the exact bit error probability.

Finally, we can observe the following from Fig. 5: (i) improvement of M-ary AC-FSK energy efficiency is evident when M is increased from 16 to 128 (i.e., to reach a given BER, the required $E_{\mathrm{b(opt)}}/N_0$ is reduced when M is increased); (ii) the theoretical BER approximation is in close conformity with the Monte Carlo BER results for ML TD receiver; (iii) BER performance with 2-tap harmonic receiver is almost the same as the one with optimal TD ML receiver, with a deviation of no more than 5%; and (iv) 1-tap DCT-based receiver has degraded BER performance as compared to optimal TD ML receiver, i.e., it requires approximately 1 dB higher $E_{\mathrm{b(opt)}}/N_0$ to reach a target BER of 10^{-3}.

D. Spectral efficiency versus Energy efficiency performance

Fig. 6 illustrates the simulation results of spectral efficiency η versus the required $E_{\mathrm{b(opt)}}/N_0$ to target a BER of 10^{-3}, for an AWGN and considering: i) M-ary AC-FSK with 2-tap harmonic receiver, ii) M-ary U-FSK with $(12, 2)$-tap harmonic receiver, iii) OOK with optimal ML receiver, iv) M-ary PAM with optimal ML receiver. From Fig. 6, it can be

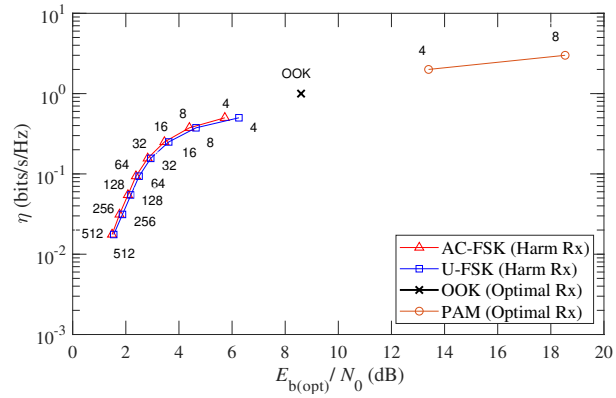

Fig. 6: Spectral efficiency η versus required $E_{\mathrm{b(opt)}}/N_0$ to target a BER of 10^{-3} for M-ary AC-FSK, M-ary U-FSK, OOK and M-ary PAM.

TABLE II: Experimental parameters to evaluate the performance of M-ary AC-FSK and M-ary U-FSK.

	AC-FSK / U-FSK	
Dictionary size, M	16	128
Sampling Frequency, F_{s} (MHz)	25	25
Oversampling Ratio, K	4	4
Bandwidth, B (MHz)	3.125	3.125
Data Rate, R_{b} (Mbit/s)	0.78	0.17
Spectral Efficiency, η (bit/s/Hz)	0.25	5.4×10^{-2}

seen that the 2-tap harmonic receiver based M-ary AC-FSK has slightly better performance than the $(12, 2)$-tap harmonic receiver based M-ary U-FSK because of slightly larger penalty factor γ, leading to a slightly improved energy efficiency (cf. section II.B). For any target spectral efficiency $\eta \leq 0.4$ bit/s/Hz, we need about 0.1 dB less $E_{\mathrm{b(opt)}}/N_0$ for M-ary AC-FSK as compared to M-ary U-FSK. Moreover, we can clearly see from Fig. 6 that energy efficiency is improving by increasing M at the expense of reducing spectral efficiency for M-ary AC-FSK and M-ary U-FSK. Performance of M-ary PAM and OOK (special case of M-ary PAM with $M = 2$) have also been reported in Fig. 6. Recall that the spectral efficiency of the M-ary PAM is $\log_2(M)$ (bits/s/Hz) [19] [10]. The performance of OOK and 4 PAM are worse than 4 AC-FSK of about 2.9 dB and 7 dB, respectively. Since M-ary PAM is a linear modulation, we can clearly see on Fig. 6 the typical degradation of energy efficiency when increasing modulation order M.

IV. Experimental Results

A. Experimental Test Bench

Fig. 7 (a) illustrates the experimental setup of the IM-DD VLC system. The test-bench is built from commercial off-the-shelf (COTS) devices [20]. The VLC transmitter (TX) (cf. Fig. 7 (b)) uses a Red Green Blue Amber (RGBA) LED (LED Engin LZA-00MA00) which integrates 4 chips (one per colour). The LED viewing angle is 95° (full opening

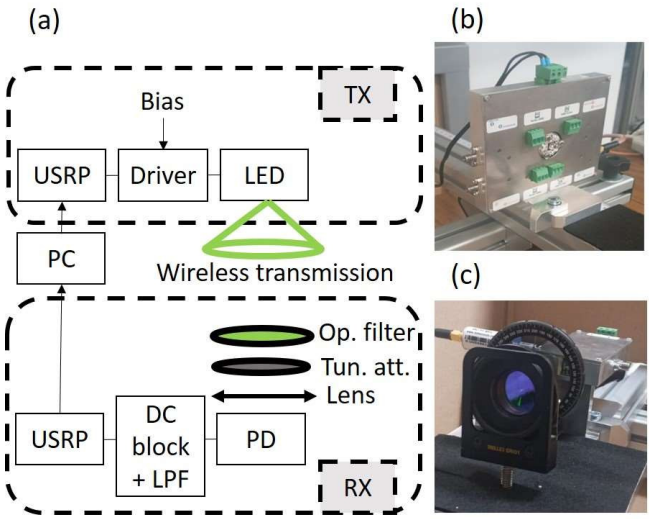

Fig. 7: Experimental setup for M-ary AC-FSK VLC system (a), LED transmitter (driver and LED) (b), receiver (c). Op. filter: optical filter, Tun. att.: tunable attenuator.

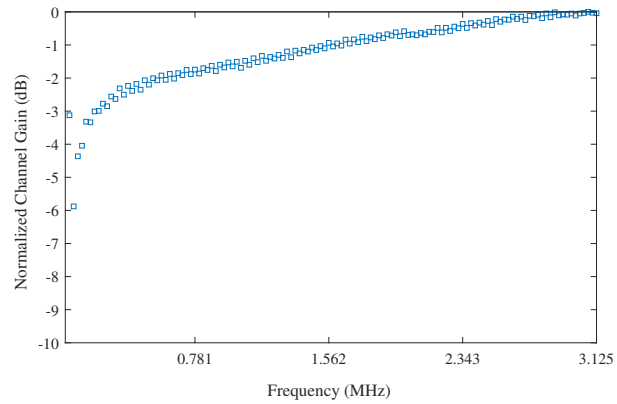

Fig. 8: Measured normalized channel gain over bandwidth B=3.125 MHz.

angle at 50% maximum intensity). Only green colour with an emitted wavelength $\lambda = 525$ nm is modulated for our VLC experiment. A dedicated LED driver has been designed to reach an available modulation bandwidth of about 10 MHz. LED bias is set at 200 mA in a relatively linear region of the LED Light-Intensity (L-I) curve, and modulation depth is adjusted to guarantee that the clipped samples amplitude of AC-FSK waveforms (cf. Fig. 1) corresponds to the zero-level optical intensity. The emitted surface power density of the LED, $\rho_{\mathrm{t(opt)}}$ is evaluated as 1.7mW/cm^2. The optical channel is line-of-sight (LOS) and the distance between the emitter and the receiver is fixed to 1 m. At the receiver (cf. Fig. 7 (c)), a green optical filter (Thorlabs FD1D) is used to filter out unwanted wavelengths from ambient light. It is followed by a tunable optical attenuator (Thorlabs NDC-50C-2M-A) to evaluate the VLC system performance under different received optical powers, $P_{\mathrm{r(opt)}}$. A silicon PIN photodiode (PD) (Hamamatsu S10784), which integrates a focusing lens, realizes direct conversion of the intensity modulation into electrical modulation. The effective photosensitive area is 7 mm^2, PD responsivity is approximately 0.35 A/W at $\lambda = 525$ nm and PD electrical bandwidth is of about 200 MHz. The PD is followed by a DC block to remove any DC offset induced by the parasitic ambient light detection. Then, a low-pass filter (LPF) with a cut-of-frequency of about 12 MHz is used as an anti-aliasing filter before analog-to-digital conversion and demodulation. For digital modulation and demodulation capabilities, a software-defined-radio (SDR) equipment (Ettus Research USRP N210) is used. SDR is interfaced with MATLAB for modulator/demodulator digital signal processing implementation [21], with the perspective of comparing the performance of AC-FSK with state-of-the-art U-FSK modulation scheme, implementing our different receiver architectures (cf. section II.D). Baseband front-ends (Ettus LFTX and LFRX daughter boards) are mounted on USRP N210 platform for digital-to-analog and analog-to-digital conversions ($0 - 30$ MHz bandwidth). Details about USRP sampling frequency (F_{s}), oversampling ratio (K), modulation signal bandwidths (B), data rates (R_{b}) and spectral efficiencies (η), are reported in Tab. II.

B. Channel Response

To estimate the channel gain of the VLC system, a frame of M-ary FSK symbols with carrier frequency increasing from $1/2T_s$ to $(M-1)/2T_s$ is generated with USRP ($F_{\mathrm{s}} = 25$ MHz, $K = 4$) and sent to the LED driver. A simple DC bias is added to the FSK symbols to make them unipolar. M is set at 128 and the occupied bandwidth by all FSK symbols is $B = 3.125$ MHz, which is the same as AC-FSK and U-FSK bandwidth (cf. Tab. II). After optical wireless transmission and photodetection, a DCT is operated on each FSK symbol, which gives an estimate of the channel magnitude response, $|H(f)|$ at each FSK symbol frequency. It has to be noticed that channel response includes LED driver response, wireless channel response and optical receiver response. Fig. 8 shows the obtained normalized channel gain of the VLC system over bandwidth B, plotted in Decibel unit (dB), $i.e.$, $20.\log(|H(f)|)$. As it can be seen on Fig. 8, the channel gain has a high pass filtering behaviour with a moderate slope (about 6 dB variation in the global bandwidth). It has been identified that this behaviour is mainly induced by the LED driver which includes a bias tee to combine the digitally modulated current with the DC bias current to feed the LED. This bias tee integrates a serial capacitance on its RF port for DC decoupling purpose, which acts as a high pass filter.

C. Bit-error-rate (BER) Performance

In this subsection, an overview of the experimental results of the proposed M-ary AC-FSK relative to State-of-The-Art M-ary U-FSK is provided. Theoretical approximation in (20) is also presented as a benchmark. Experimental BER results for OOK have not been reported as benchmark, because our channel frequency response (high pass filtering effect shown in Fig. 8) strongly affects OOK baseband spectrum. As a consequence, OOK BER is very degraded.

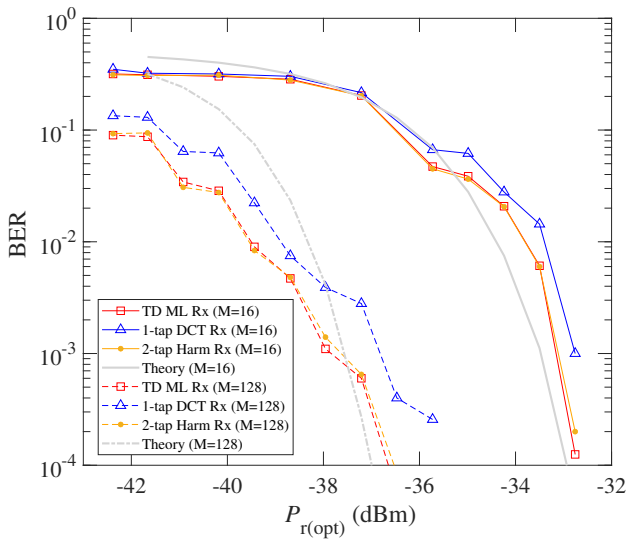

Fig. 9: Experimental and theoretical approximation (Theory) for BER performance against $P_{\mathrm{r(opt)}}$ for M-ary AC-FSK receivers, considering $M = \{16, 128\}$

.

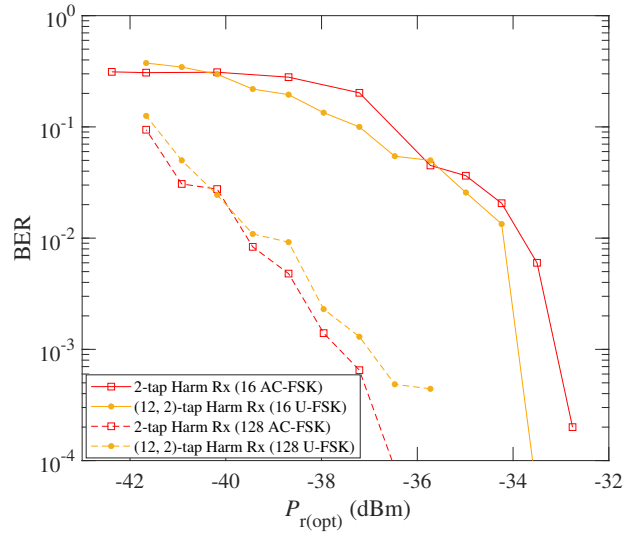

Fig. 10: Experimental BER performance against $P_{\mathrm{r(opt)}}$ of the L-tap harmonic receiver (Harm Rx) for M-ary AC-FSK and M-ary U-FSK, considering $M = 16$ & 128.

Experiments are performed in an optical line-of-sight (LOS) channel with pre-defined modulation at transmitter side, and real-time demodulation at receiver side. BER measurements are realized by counting a minimum of 100 bit errors to ensure sufficient BER accuracy.

Fig. 9 depicts the experimental BER performance against the received optical power, $P_{\mathrm{r(opt)}}$ using the optimal TD ML receiver, the 1-tap DCT-based receiver or the 2-tap harmonic receiver over optical LOS channel, while considering $M = \{16, 128\}$ AC-FSK. Fig. 9 shows the improved energy efficiency when increasing AC-FSK modulation order at an expense of spectral efficiency (cf. Tab. II). This is because the minimum distance between the symbol pairs increases by increasing M, since d^2_{min} is proportional to the symbol energy $E_{\mathrm{s(elec)}}$ for this modulation, with a proportionality constant independent on M (cf. (7)). As a consequence, for a given $E_{\mathrm{s(elec)}}/N_0$ ratio, BER is identical for any dictionary size. Since $E_{\mathrm{b(elec)}} = E_{\mathrm{s(elec)}}/\log_2(M)$ with $\lambda = \log_2(M)$ the number of bits per symbol, BER as a function of $E_{\mathrm{b(elec)}}/N_0$ is improved when λ is increased. This result is counter-intuitive when considering linear modulations, but it is a common behavior when considering (orthogonal) non-linear modulations [12][13][6].

From Fig. 9, it can be seen that the optimal TD ML receiver has better BER performance than 1-tap DCT-based receiver, which was expected (see section II.D). The necessary $P_{\mathrm{r(opt)}}$ for TD ML receiver to achieve a BER value of 10^{-3} is 1 dB lower than the necessary $P_{\mathrm{r(opt)}}$ to achieve the same BER value using 1-tap DCT receiver. This result is compliant with Fig. 5 considering that the noise power spectrum density, N_0 is supposed to be independent from $P_{\mathrm{r(opt)}}$ (N_0 is mainly induced by thermal noise, ambient noise and receiver circuit noise figure). From Fig. 9, it can also be observed that the 2-tap harmonic receiver shows the same BER performance as the optimal TD ML receiver, with a complexity reduction of about 56.3% (respectively 92.2%) for $M = 16$ (respectively $M = 128$). These similar BER measurements are compliant with simulation results shown in Fig. 5. Theoretical approximation (20) has been reported on Fig. 9. For calibrating $E_{\mathrm{b(opt)}}/N_0$ in the theoretical bit error probability (20) relatively to $P_{\mathrm{r(opt)}}$, $E_{\mathrm{b(opt)}}$ and $P_{\mathrm{r(opt)}}$ are related using $E_{\mathrm{b(opt)}} = P_{\mathrm{r(opt)}}T_{\mathrm{b}}$. $T_{\mathrm{b}} = 1/R_{\mathrm{b}}$ is extracted from Tab. II and is used also to explicit Γ parameter definition (see (19)) used in (20). Then, a N_0 value of -160 dBm/Hz is found so that the bit error probability reaches a value of 10^{-3} for the optical power $P_{\mathrm{r(opt)}} = -36.7$ dBm for $M = 16$, in order to fit approximately the experimental BER result of Fig. 9. In the following step, maintaining the same value $N_0 = -160$ dBm/Hz, the theoretical bit error probability is computed for $M = 128$ as a function of $P_{\mathrm{r(opt)}}$ using (20). Theoretical bit error probabilities for $M = \{16, 128\}$ match relatively well with TD ML and harmonic receivers experimental results. Slight differences between theoretical bit error probabilities and BER measurements may come from the channel frequency response, which is not perfectly flat, as shown on Fig. 8.

Fig. 10 illustrates the experimental BER performance against received optical power, $P_{\mathrm{r(opt)}}$ considering L-tap harmonic receiver for M-ary AC-FSK and M-ary U-FSK [15] with modulation orders $M = \{16, 128\}$. In the harmonic receiver, only $L = 2$ taps are considered for all AC-FSK frequency waveforms [16], whereas $L_{\mathrm{o}} = 2$ and $L_{\mathrm{e}} = 12$ taps are used for odd and even U-FSK frequency waveforms, respectively [15]. It can be seen in Fig. 10 that the measured BER performance of M-ary AC-FSK is similar as the one of M-ary U-FSK for $M = 16$. For $M = 128$, slightly degraded performance can be observed for U-FSK relatively to 128 AC-FSK, which may come from the impact of the receiver low pass filtering (cf Fig. 7) on the numerous U-FSK waveform harmonics. Moreover, AC-FSK harmonic receiver complexity

is found to be 41.6% (respectively 33.3%) lower than U-FSK harmonic receiver complexity for $M = 16$ (respectively $M = 128$), due to the limited number of taps used in AC-FSK harmonic receiver (see section II.D).

V. Conclusion

In this article, theoretical analysis and experimental demonstration of AC-FSK are presented for low data rate and energy efficient VLC. AC-FSK signalling is introduced and different receiver architectures are succinctly described. Euclidean distance analysis between AC-FSK waveforms leads us to an approximate expression of theoretical bit error probability as a function of received average optical energy per bit to allow a straightforward comparison with experimental results. The VLC test-bench, composed of COTS devices interfaced with SDR equipment is presented, and VLC channel gain is measured. BER measurements show approximately similar results as theoretical results and the improvement of AC-FSK energy efficiency is experimentally demonstrated when increasing modulation order M from 16 to 128. BER measurement comparisons between 3 different receivers show that harmonic receiver has similar performance as TD ML receiver with the benefit of a drastically reduced complexity. Performance comparison between AC-FSK and U-FSK signalling using harmonic receiver reveals that both modulations reach similar BER. However, AC-FSK harmonic receiver shows significantly reduced complexity relatively to U-FSK harmonic receiver due to the reduced number of taps in frequency-domain AC-FSK waveforms. A perspective of this work is to investigate efficient coding schemes associated with AC-FSK modulation technique to improve even further AC-FSK energy efficiency for low data rate VLC systems.

References

[1] C.-W. Chen, W.-C. Wang, J.-T. Wu, *et al.*, "Visible light communications for the implementation of internet-of-things," *Optical Engineering*, vol. 55, no. 6, p. 060 501, 2016.

[2] H. Haas, L. Yin, Y. Wang, and C. Chen, "What is LiFi?" *Journal of lightwave technology*, vol. 34, no. 6, pp. 1533–1544, 2015.

[3] A. Nuwanpriya, S.-W. Ho, J. A. Zhang, A. J. Grant, and L. Luo, "PAM-SCFDE for optical wireless communications," *Journal of Lightwave Technology*, vol. 33, no. 14, pp. 2938–2949, 2015.

[4] S. D. Dissanayake and J. Armstrong, "Comparison of ACO-OFDM, DCO-OFDM and ADO-OFDM in IM/DD systems," *Journal of lightwave technology*, vol. 31, no. 7, pp. 1063–1072, 2013.

[5] B. Béchadergue, L. Chassagne, and H. Guan, "Suitability of visible light communication for platooning applications: An experimental study," in *2018 Global LIFI Congress (GLC)*, IEEE, 2018, pp. 1–6.

[6] J. G. Proakis and M. Salehi, *Digital communications*. McGraw-Hill., 2008.

[7] H. Park and J. R. Barry, "Trellis-coded multiple-pulse-position modulation for wireless infrared communications," *IEEE transactions on communications*, vol. 52, no. 4, pp. 643–651, 2004.

[8] H.-J. Jang, J.-H. Choi, Z. Ghassemlooy, and C. G. Lee, "PWM-based PPM format for dimming control in visible light communication system," in *2012 8th International Symposium on Communication Systems, Networks & Digital Signal Processing (CSNDSP)*, IEEE, 2012, pp. 1–5.

[9] A. Pradana, N. Ahmadi, T. Adiono, W. A. Cahyadi, and Y.-H. Chung, "VLC physical layer design based on pulse position modulation (PPM) for stable illumination," in *2015 international symposium on intelligent signal processing and communication systems (ISPACS)*, IEEE, 2015, pp. 368–373.

[10] A. W. Azim, A. Rullier, Y. Le Guennec, L. Ros, and G. Maury, "Energy efficient M-ary frequency-shift keying-based modulation techniques for visible light communication," *IEEE Transactions on Cognitive Communications and Networking*, vol. 5, no. 4, pp. 1244–1256, 2019.

[11] C. Manimegalai, S. Gauni, N. Raghavan, and T. R. Rao, "Investigations on suitable modulation techniques for visible light communications," in *2017 International Conference on Wireless Communications, Signal Processing and Networking (WiSPNET)*, IEEE, 2017, pp. 1818–1822.

[12] Y. Roth, J.-B. Doré, L. Ros, and V. Berg, *The Physical Layer of Low Power Wide Area Networks: Strategies, Information Theory's Limit and Existing Solutions*. Advances in Signal Processing: Reviews, vol. 1, Book Series, 2018.

[13] ——, "Turbo-FSK, a physical layer for low-power wide-area networks: Analysis and optimization," *Comptes Rendus Physique*, vol. 18, no. 2, pp. 178–188, 2017.

[14] A. W. Azim, Y. Le Guennec, and L. Ros, "Hybrid frequency and phase-shift keying modulation for energy efficient optical wireless systems," *IEEE Wireless Communications Letters*, vol. 9, no. 4, pp. 429–432, 2019.

[15] A. Azim, M. Khan, O. De Wulf, Y. Le Guennec, G. Maury, and L. Ros, "Near-optimal low-complexity harmonic receiver for Unipolar-FSK," *IEEE Wireless Communications Letters*, 2021.

[16] M. J. Khan, A. W. Azim, Y. Le Guennec, G. Maury, and L. Ros, "Asymmetrically clipped-FSK modulation for energy efficient visible light communications," in *2021 IEEE 32nd Annual International Symposium on Personal, Indoor and Mobile Radio Communications (PIMRC)*, IEEE, 2021, pp. 458–464.

[17] S. Mazahir, A. Chaaban, H. Elgala, and M.-S. Alouini, "Achievable rates of multi-carrier modulation schemes for bandlimited IM/DD systems," *IEEE Transactions on Wireless Communications*, vol. 18, no. 3, pp. 1957–1973, 2019.

[18] J. Armstrong and B. J. Schmidt, "Comparison of asymmetrically clipped optical OFDM and DC-biased optical OFDM in AWGN," *IEEE Communications Letters*, vol. 12, no. 5, pp. 343–345, 2008.

[19] Z. Ghassemlooy, W. Popoola, and S. Rajbhandari, *Optical wireless communications: system and channel modelling with Matlab®*. CRC press, 2019.

[20] F. Wu, C.-T. Lin, C. Wei, *et al.*, "Performance comparison of OFDM signal and CAP signal over high capacity RGB-LED-based WDM visible light communication," *IEEE Photonics Journal*, vol. 5, no. 4, pp. 7 901 507–7 901 507, 2013.

[21] J. Baranda, P. Henarejos, and C. G. Gavrincea, "An SDR implementation of a visible light communication system based on the IEEE 802.15. 7 standard," in *ICT 2013*, IEEE, 2013, pp. 1–5.